AIP | Review of Scientific Instruments

Absolute photo-destruction and photo-fragmentation cross section measurements using an electrostatic ion beam trap

O. Aviv, B. Kafle, V. Chandrasekaran, O. Heber, M. L. Rappaport, H. Rubinstein, D. Schwalm, D. Strasser, Y. Toker, and D. Zajfman

Citation: Review of Scientific Instruments **84**, 053106 (2013); doi: 10.1063/1.4804646
View online: http://dx.doi.org/10.1063/1.4804646
View Table of Contents: http://scitation.aip.org/content/aip/journal/rsi/84/5?ver=pdfcov
Published by the AIP Publishing

Absolute photo-destruction and photo-fragmentation cross section measurements using an electrostatic ion beam trap

O. Aviv,[1] B. Kafle,[1] V. Chandrasekaran,[1] O. Heber,[1] M. L. Rappaport,[1] H. Rubinstein,[1] D. Schwalm,[1,2] D. Strasser,[3] Y. Toker,[1] and D. Zajfman[1]
[1]*Department of Particle Physics and Astrophysics, Weizmann Institute of Science, Rehovot 76100, Israel*
[2]*Max-Planck-Institut für Kernphysik, D-69117 Heidelberg, Germany*
[3]*Institute of Chemistry, Hebrew University of Jerusalem, 91904 Jerusalem, Israel*

(Received 27 March 2013; accepted 29 April 2013; published online 15 May 2013)

We describe a technique to measure absolute photo-induced cross sections for cluster anions stored in an electrostatic ion beam trap (EIBT) with a central deflector. The setup allows determination of total photo-destruction cross sections as well as partial cross sections for fragmentation and electron detachment. The unique properties of this special EIBT setup are investigated and illustrated using small Al_n^- clusters. © *2013 AIP Publishing LLC*. [http://dx.doi.org/10.1063/1.4804646]

I. INTRODUCTION

Since the first realization of an electrostatic ion beam trap (EIBT) by Zajfman *et al.* in the late 1990s,[1,2] this compact trapping device has found its way into many laboratories around the world as a convenient tool to study fundamental properties of atomic, molecular, and cluster ions.[3] In its basic design, the EIBT consists of two electrostatic mirrors between which ions with kinetic energies of several keV oscillate back and forth. The trap combines storage times of the order of seconds with a straight, field-free region, which makes it ideally suited for merged or crossed beam experiments. Experiments are drawing additional advantages from the high kinetic energy and directionality of the reaction products, which facilitate their effective detection. A few among the recent developments of this device are: The realization of an EIBT employing liquid helium cooling to reach extremely low blackbody radiation temperatures of $\lesssim$15 K and residual gas densities allowing for storage times of up to 5 min, unprecedented for keV ion beams.[4] Johnson and Continetti[5] combined a cryogenic EIBT with a velocity mapping electron spectrometer to study the dynamics of chemical reactions by photoelectron-photofragment coincidences. The ability to extract high resolution mass spectra from these traps has been enhanced by an order of magnitude by employing a new analysis method, which samples the ion oscillation data with a comb-like function instead of using the standard Fourier technique.[6] And most recently, a new project has been launched[7] to study the β-decay of light radioactive nuclei by electron-recoiling-ion coincidences in an EIBT, taking advantage of the field-free decay volume and the kinematic focusing of the recoiling nucleus characteristic of this trapping technique.

We have recently extended the standard linear EIBT configuration by introducing a spherical electrostatic deflector in the center of the trap, that can bend the stored ions by 33° towards a third electrostatic mirror such that they oscillate on V-shaped trajectories.[8,9] The stored ions pass through a central hole in a position-sensitive micro-channel plate (MCP) that is located between the deflector and the third mirror. In this bent version, all of the advantages of the linear EIBT are retained, but due to the dispersion introduced by the deflector, charged photo-fragments produced in front of the deflector are separated from the ion beam and can be identified according to their mass with the position sensitive MCP. This unique property of the bent EIBT has been used, e.g., in a systematic investigation of the competition between delayed electron and delayed atom emission from photo-excited Al_4^- clusters.[10]

The bent EIBT, being an optimized configuration for delayed emission studies, is suited neither for measuring the prompt contributions to the laser-induced reaction yields nor for determining absolute cross sections. However, the bent EIBT allows the storage of ions also in a linear configuration, which—together with the deflector—opens up a unique possibility to measure absolute photo-destruction cross sections and to determine total partial cross sections into individual fragmentation channels.

In these measurements, the third mirror is not used. Here the clusters are first stored on linear trajectories by grounding the deflector so that all ions can be well overlapped with a pulsed coaxial laser beam. After the laser pulse, a fast voltage step is applied to the deflector electrodes to guide a fraction of the remaining clusters (or of the charged fragments produced) out of the trap towards an MCP located after the grounded third mirror. Counting the clusters—alternately for consecutive injections—before and after the laser pulse, the survival probability $P(U)$ and thus the depletion $D(U) = 1 - P(U)$ can be determined as a function of the laser pulse energy U, from which the absolute photo-destruction cross section σ_0 can be deduced. Similarly, by switching the deflector voltage simultaneously with (after) the laser pulse to a value required to guide charged fragments produced in the fragmentation channel f to the detector, the prompt (delayed) appearance probabilities $P_f(U)$ of the fragment can be measured, from which the fragmentation cross section σ_f can be determined.

The measurement and analysis of absolute cross sections required several additional technological investigations to take full advantage of this application of the bent EIBT. They are discussed in the present paper (Sec. II) together with selected results obtained with Al_n^- anions to exemplify the measurement procedures and the analysis of depletion curves and

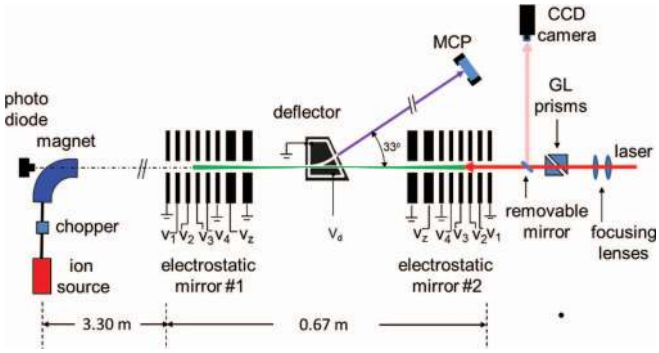

FIG. 1. Schematic view of the experimental setup.

fragment appearance curves in terms of absolute destruction (Sec. III) and fragmentation cross sections (Sec. IV). A detailed study of absolute cross sections for Al_4^- as a function of laser wavelengths will be presented in a forthcoming publication.[11]

II. EXPERIMENTAL ISSUES

A. Experimental setup

A schematic view of the experimental setup used in the present study is shown in Fig. 1. Negatively charged aluminum clusters Al_n^- are produced in a cesium sputter ion source and accelerated to a kinetic energy of 4.2 keV. The ions are bunched by an electrostatic chopper at the exit of the ion source, mass selected by a magnet, and then steered and focused into the trap chamber where they are stored between the two electrostatic mirrors of the linear EIBT configuration. The electrostatic deflector is mounted in the middle of the trap, and with both its electrodes grounded, the ions can pass freely through the 3.0 mm diameter hole in the concave electrode if the mirror voltages are carefully adjusted. By optimizing the lifetimes of the ions in the trap these voltages were found to be $(V_1, V_2, V_3, V_4, V_Z) = (-6.477, -4.875, -3.900, -1.050, -4.110)$ kV. At these settings the lifetimes of Al_n^- clusters were observed to be solely limited by residual gas scattering and to result in typical lifetimes of $\sim$1 s at a residual gas pressure of 3×10^{-10} mbar.

The stored cluster beam can be overlapped by short laser pulses ($\tau_l \sim 9$ ns), that are generated by an optical parametric oscillator (model NT342 by EKSPLA) with wavelengths tunable between 210 and 2600 nm and line widths of $\sim$0.1 nm. The repetition rate of the laser is 10 Hz but can be decreased if required using a mechanical shutter. The laser beam is passed through a telescope and carefully adjusted along the z axis of the setup by optimizing the transmission through the deflector hole. A Glan-Taylor polarizing prism (model GT10 by Thorlabs) is used to vary the energy of the laser pulse. The laser beam profile is adjusted and controlled by inserting a mirror into the optical path and observing the profile by a CCD camera mounted at a distance corresponding to the distance of the mirror to the middle of the trap. The pulse energy transmitted through the deflector hole is measured for each laser pulse by a photo-diode (model RjP-637 by Laser Probe) located after the bending magnet about $\sim$4 m upstream of the EIBT. The photo-diode has an active area of 10 mm diameter, which is at least twice as large as the width of the impinging laser spot-size. The measured pulse energy had to be increased by 5% to account for the reflection of the laser beam at the exit window of the vacuum chamber of the bending magnet.

Applying a voltage step to the concave electrode of the deflector, clusters located (charged fragments created) in front of the deflector can be extracted from the trap and detected by a MCP detector of 25 mm diameter, mounted at a distance of 125 cm from the trap center. As the deflector voltage required to guide the original clusters of mass m_p to the MCP amounts to $V_{def} = V_p = 1.580$ kV, the required deflector voltage to properly deflect charged daughter fragments of mass m_f towards the MCP is thus given by $V_{def}(m_f) = (m_f/m_p)V_p$.

The micro-channel plate detector is also equipped with a phosphor screen which can be observed by a CCD camera to monitor the spatial distribution of the deflected particles on the MCP. These distributions are found to be well contained within the active area of the detector. Moreover, from the measured V_{def} dependence of the count rate one estimates that daughter fragments can be safely distinguished from parent ions if $(m_p - m_f)/m_p \gtrsim 0.05$, that is, X_{n-1}^- daughter fragments are well separated from the X_n^- parent ions as long as $n \lesssim 20$.

B. Ion density

The interpretation of the reaction rates between clusters and photons requires the knowledge of the volume density $N_0\rho(z, r)$ of the stored ions, where N_0 is the total number of ions stored and $\rho(z, r)$ denotes the (normalized) probability to find an ion in the volume element $rdrd\varphi dz$, which is preferentially described in cylindrical coordinates to take advantage of the symmetry of the density around the trap's z axis. Since the trap is operated in the non-bunching mode, we expect that the bunch injected into the trap will uniformly fill the trap after a few ms of storage.[12]

Monte Carlo simulations were performed to derive the volume density using the SIMION program package[13] together with a detailed geometric description of the trap and the specific setting of the mirror voltages. The main panel of Fig. 2 displays the number of particles per unit length when integrating the simulated volume density distribution over r and φ. The pattern of the z-projection reflects the slowing down of the ions in the Einzel lens and in the mirror electrodes: the probability to find the ion between z and $z + dz$ is proportional to the time it spends in dz, which in turn is inversely proportional to the z-component of the velocity at z. The inset displays the r-dependence of the density distribution for three different z-regions. They show that the ions are transversely well-localized at all z-positions; even within the Einzel lenses of the mirrors, where the tail of the transversal distribution is getting most pronounced (blue squares in Fig. 2), the majority of the clusters is still located within a radius of 1.5 mm around the trap axis.

C. Laser beam profile

A typical laser beam profile observed with the CCD camera for a single laser shot is shown in Fig. 3. Although the

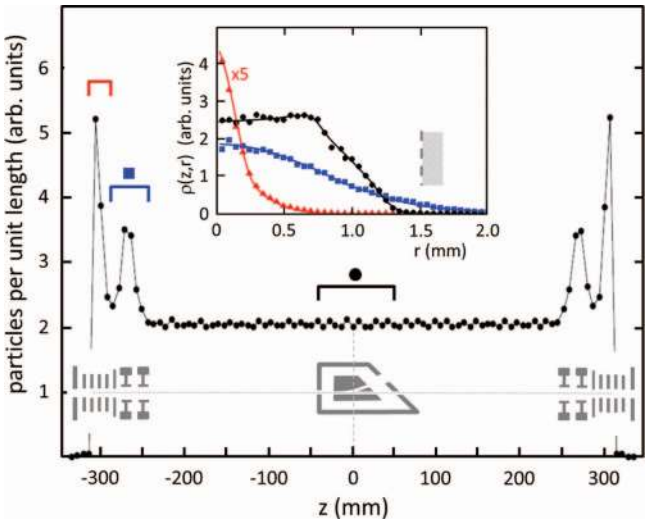

FIG. 2. Main panel: Projection of the volume density of stored ions derived by Monte Carlo simulations onto the trap axis. Inset: r-dependence of the simulated volume density for three different z-regions; inside the deflector (black circles), inside the Einzel lens (blue squares), and inside the outer mirror electrodes (red triangles). The radius of the deflector hole (1.5 mm) is indicated by the dashed gray line.

profile shapes fluctuate in details from shot to shot, the average profile can be reasonably well represented by a symmetric Gaussian profile characterized by a variance σ_l. Moreover, in view of the large focal length of the telescope used to form the laser beam, the variance can be assumed to be constant over the length of the trap. We, therefore, describe the number of photons transversing the area element $rdrd\varphi$ perpendicular to the trap axis by

$$n_{ph}(r) = N_{ph} f(r), \tag{1}$$

where N_{ph} denotes the number of photons in the laser pulse, and the (normalized) area density $f(r)$ is given by

$$f(r) = \frac{1}{2\pi\sigma_l^2} \exp\left(-r^2/2\sigma_l^2\right). \tag{2}$$

While σ_l can be assumed to be constant over the length of the trap, the laser beam is collimated after passing through the deflector to $r \le r_0$, where $r_0 = 1.5$ mm denotes the radius of the deflector hole.

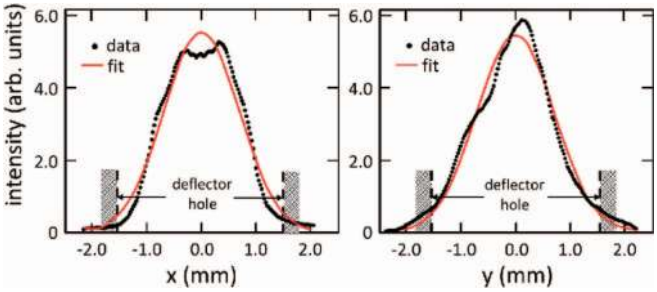

FIG. 3. A typical laser beam profile at the center of the trap, obtained by projecting the two-dimensional intensity distribution measured with the CCD camera for a single laser shot onto the x axis (left panel) and onto the y axis (right panel), respectively. The solid (red) lines are Gaussian fits assuming a variance of $\sigma_l = 0.7$ mm, which corresponds to a FWHM of 1.65 mm.

The number of photons in the laser pulse is readily obtained from the laser pulse energy U transmitted through the deflector and measured for each pulse by the photo-diode, namely,

$$N_{ph} = \frac{U}{\hbar\omega}\frac{1}{Q(r_0)}, \quad \text{with} \quad Q(r_0) = 2\pi\int_0^{r_0} f(r) r dr, \tag{3}$$

where $\hbar\omega$ denotes the energy of the photons.

D. Detection efficiencies

The number of stored clusters (charged fragments produced by a laser pulse) can be deduced from the number of ions recorded by the MCP detector after the deflector voltage has been raised to the value appropriate to deflect parent clusters ($\mu = p$) or daughter fragments ($\mu = f$). This requires the knowledge of the overall detection efficiency ϵ_μ, which is determined by two contributions, (i) by the collection efficiency ϵ_μ^{col}, i.e., the percentage of ions (fragments produced) that can actually be transported to the MCP, and (ii) by the recording efficiency ϵ_μ^{rec}, i.e., the probability that an ion hitting the MCP actually produces an output signal, that is,

$$\epsilon_\mu = \epsilon_\mu^{col}\epsilon_\mu^{rec}. \tag{4}$$

The recording efficiencies for the MCP detector in use were determined previously and are compiled in Ref. 9 (MCP #3). The collection efficiencies for parent clusters and fragments, however, require extra attention.

1. Collection efficiency of parent clusters

For parent clusters, the collection efficiency can be readily determined from the ratio of the spill time $T_{spill,p}$, i.e., the length of the pulse train arriving at the MCP, to the oscillation time T_{osc} of the clusters in the trap,

$$\epsilon_p^{col} = T_{spill,p}/T_{osc}. \tag{5}$$

Spill times were measured for Al_n^- clusters with $2 \le n \le 8$ and were found to be well described by

$$T_{spill,p} = 0.445 T_{osc} - \delta t_{def}. \tag{6}$$

The proportionality factor of 0.445 was determined from Monte Carlo simulations of the collection efficiency assuming the rise time of the voltage step applied to the deflector to be infinitely short; the factor agrees well with what is expected from simple geometric considerations (see Fig. 4), namely, that only those clusters can be properly deflected that are moving from the grounded shield of the deflector towards the entrance mirror (mirror #1) and back towards the deflector, i.e., which are located between points marked as z_a^- and z_e^- in Fig. 4 at the moment the deflector is switched. The constant offset of $\delta t_{def} = 0.60\,\mu$s is due to the finite rise time of the deflector voltage, which causes a fraction of the ions in front of z_e^- not to be properly deflected.

For Al_4^- of 4.2 keV one finds, for example, $T_{osc} = 16.0\,\mu$s, $T_{spill,p} = 6.6\,\mu$s, and $\epsilon_p^{col} = 0.41$. The collection efficiencies determined for 4.2 keV Al_n^- clusters from measured spill times are displayed in Fig. 4 together with the expectation using Eq. (6) (referred to as schematic model).

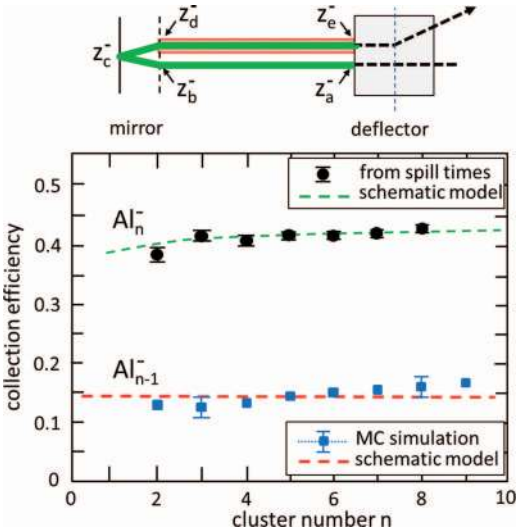

FIG. 4. Upper panel: Definition of the positions z_a^- to z_e^- used in the schematic model approach to the collection efficiencies. At z_a^- and z_e^-, ions are leaving and re-entering the grounded shield of the deflector, while at z_b^- and z_d^- they are entering and leaving the inner grounded electrode of the Einzel lens of the entrance mirror, respectively. Within this model approach clusters stored between z_a^- and z_e^- at the moment the deflector voltage is switched (thick (green) line) can be deflected towards the MCP, while only fragments created between z_d^- and z_e^- (dashed (red) line) can be detected by the MCP. Lower panel: Collection efficiencies for Al_n^- parent clusters (black dots) and Al_{n-1}^- daughter fragments (blue squares) as a function of cluster number n. For parent clusters, the efficiencies are derived from measured spill times using Eq. (5) while the fragment efficiencies were determined by Monte Carlo simulations. Also shown are the collection efficiencies expected within the schematic model (Eqs. (6) and (7); dashed lines).

2. Collection efficiency of fragments

As photo-induced fragments have lower masses and thus lower kinetic energies than the parent ions, fragments do not remain stored if the energy difference between parent and daughter is larger than the acceptance range of the trap, i.e., if the energy change $(E_p - E_f)/E_p = (m_p - m_f)/m_p$ is larger than ~5%.[14] Thus the time difference between the laser shot and the activation of the deflector has to be properly adjusted to optimize the detection of fragments. Moreover, the expectation is that only those fragments produced between z_d^- and z_e^- (see Fig. 4) will be properly deflected towards the MCP, while fragments produced between z_a^- and z_d^- will end up on trajectories that cannot pass the deflector or miss the detector due to the different focusing properties of the mirror for less energetic ions.

In Fig. 5, the number of $n-1$ photo-fragments observed when subjecting Al_2^- and Al_4^- to photons of $\lambda = 550$ nm and 590 nm, respectively, are displayed as a function of the time difference $t = t_{def} - t_{las}$ between the onset of the deflector voltage, t_{def}, and the time of the laser shot, t_{las}. The observed time dependence is again well described by the schematic model based on geometric arguments when taking into account the finite rise time of the deflector voltage: If the deflector is switched too early, i.e., $t \le T_{a,e}$ with $T_{a,e}$ being the time of flight of the ions from z_a^- to z_e^- (see Fig. 4), no clusters will be present between between z_d^- and z_e^- when the laser is fired. On the other hand, if the deflector is activated too late, i.e., $t \ge T_{d,e} - \delta t_{def}$ with $T_{d,e}$ being the time of flight of the ions

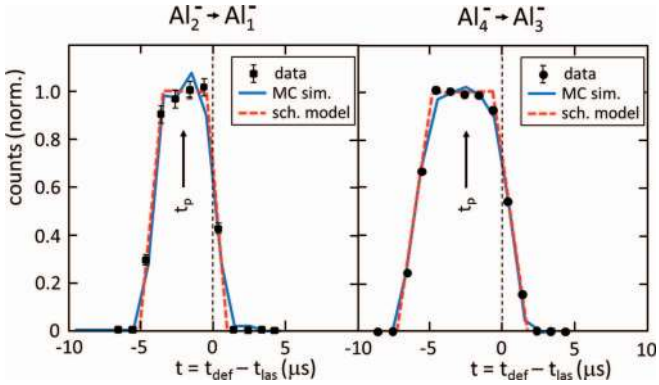

FIG. 5. Number of $(n-1)$ photo-fragments of Al_2^- (black squares, left panel) and Al_4^- (black dots, right panel) as a function of the time difference t between the onset of the deflector voltage and the time of the laser pulse (normalized to 1 at $t = t_p \approx -2.5\,\mu$s). Also shown are the expected relative collection efficiencies resulting from the schematic model (dashed red lines) and from Monte Carlo simulations (solid blue lines).

from z_d^- to z_e^-, then none of the promptly produced photo-fragments will be properly deflected. For times $-T_{b,e} < t < -\delta t_{def}$, the collection efficiency is constant and expected to be given by

$$\epsilon_f^{col} = T_{spill,f}/T_{osc} = 0.145 \tag{7}$$

as $T_{spill,f} = T_{d,e} = 0.145 T_{osc}$.

As the energy difference between Al_n^- clusters and their Al_{n-1}^- daughters is getting smaller with increasing n, the assumption that only fragments produced between z_d^- and z_e^- are collected is bound to become invalid for heavier clusters. Indeed, for Al_{n-1}^- fragments with $n \gtrsim 8$, deviations between measured and schematic model curves start to occur and Monte Carlo simulations do show that for these heavier systems also fragments produced between z_a^- and z_d^- are increasingly more likely to be collected, while for $n \lesssim 8$ excellent agreement with the schematic model prediction and the measured time distributions is observed (see Fig. 5).

Monte Carlo simulations were also used to calculate the collection efficiencies for Al_{n-1}^- fragments with $n < 10$ allowing for kinetic energy releases of up to 0.15 eV and assuming the fragmentation to be prompt within the time resolution of the setup, which corresponds to the flight time $T_{d,e}$ of the ions between z_d^- and z_e^-. The results obtained at $t = t_p \approx -2.5\,\mu$s, i.e., switching the deflector about 2.5 μs before the laser pulse to ensure optimal collection efficiencies, are compared in Fig. 4 to the prediction of Eq. (7). The simulated efficiencies are found to increase slightly from $\epsilon_f^{col} = 0.13$ for $n = 2$ to $\epsilon_f^{col} = 0.16$ for $n = 8$; within the estimated error of 10%, however, they are reasonably well accounted for by the schematic model.

The assumption that the fragmentation occurs in times that are short compared to the inherent time resolution of our setup can be verified by measuring the fragmentation yield not only at $t = t_p$ but also by delaying the switching of the deflector voltage relative to the laser pulse to times $t > T_{d,e} - \delta t_{def}$. For the measurements shown in Fig. 5 the relative yield of delayed fragmentation occurring at $t \gtrsim T_{d,e}$ can be estimated in this way to be less than 1%.

E. Dead times

The signals of the MCP detector (model E033VA with phosphor screen, active diameter 25 mm, El-Mul Technologies) used to detect the deflected ions are amplified, digitized, and recorded by a multiscaler (National Instruments PCI 6602). The multiscaler is gated by the deflector voltage with a gate length of 30 μs, which is larger than required by the spill times but sufficient to suppress MCP noise and to ensure a signal-to-noise ratio of better than 10^{-4}.

Since the particles arrive at the detector in short bunches defined by the spill time, special care was taken to minimize the total dead time τ_{dead} of the detection system and to determine its precise value. Assuming $\kappa_\mu N \ll 1$, where kappa is defined by $\kappa_\mu = \tau_{dead}/T_{spill,\mu}$ and N denotes the observed number of counts per spill, the true number N_0 of counts per spill is given to first order in $\kappa_\mu N$ by

$$N_0 = N(1 + \kappa_\mu N) \tag{8}$$

independent of the special dead time behavior (paralyzable or non-paralyzable[15]) of the detection system.

A lower limit of the dead time of $\tau_{dead} = 20$ ns was determined by feeding an electronic double pulser with a variable time delay into the preamplifier. To determine τ_{dead} also under more realistic conditions with realistic detector pulses, the dead time factor κ_p was also determined by measuring, at a constant laser pulse energy U, the laser induced depletion of Al_4^- clusters as a function of the number of injected particles (see also Sec. III). These measurements resulted in $\kappa_p = 0.0037(7)$, which—together with the known spill time of $T_{spill,p} = 6.6\,\mu$s—leads to $\tau_{dead} = 24(5)$ ns. This is the value finally adopted for performing the dead time corrections in the measurements described in Secs. III and IV. It should be noted that in view of typical spill times of several μs, the tolerable number of counts per spill are severely limited by the dead time if the relative dead time correction $\kappa_\mu N$ is to be kept below, say, 10% such that Eq. (8) stays approximately correct. For Al_4^- clusters, for example, this restriction requires N to be $\lesssim$30.

III. ABSOLUTE PHOTO-DESTRUCTION CROSS SECTIONS BY DEPLETION

In the setup described above, which ensures a comprehensive overlap of the stored particles with the laser beam, absolute photo-destruction cross sections σ_0 for ionic clusters can be determined from depletion measurements: photo-excited clusters having emitted an electron do not remain stored in the trap, and the same is true for clusters having emitted an atom or groups of atoms if the resulting energy change is larger than the acceptance range of the trap. From the number of clusters stored in the trap before and after the laser pulse, we can thus determine the survival probability $P(U)$ and the depletion probability $D(U) = 1 - P(U)$ as a function of the laser pulse energy U.

The number of stored ions is measured by switching the deflector either before or after the laser pulse to $V_{def} = V_p$. Since this measurement is destructive, the switching is done alternately before or after the laser pulse for two consecutive injections, averaging over a sufficient number of injections per pulse energy U to smooth out beam current fluctuations and to ensure adequate statistical accuracy. The number of clusters is usually measured 1 ms before and 1–2 ms after the laser pulse, respectively. The time difference between the two measurements is small enough to neglect additional cluster losses by residual gas scattering, but the waiting time after the laser pulse is sufficiently long to allow also for delayed decays to take place before the measurement, which may take a few 100 μs (see, e.g., Ref. 10). Denoting the (dead time corrected) number of clusters spilled out of the trap by switching the deflector before and after the laser pulse by N_b and N_a, respectively, the depletion function $D(U)$ is given by

$$D(U) = 1 - P(U) = 1 - \frac{N_a(U)/\epsilon_p}{N_b/\epsilon_p} = 1 - \frac{N_a(U)}{N_b}, \tag{9}$$

which is independent of the overall detection efficiency ϵ_p.

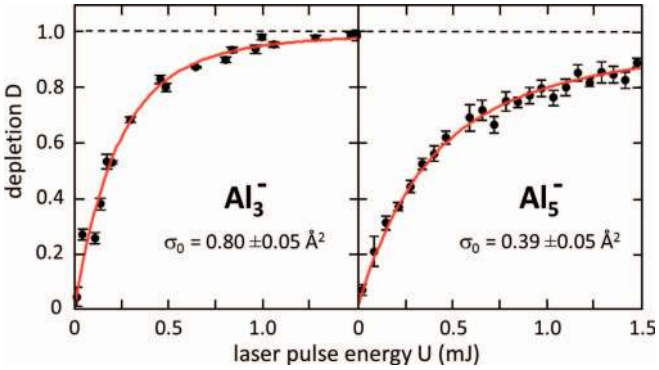

FIG. 6. Depletion curves observed for Al_3^- and Al_5^- clusters that were exposed to photons of 550 nm contained in 9 ns long laser pulses with pulse energies of up to 1.5 mJ (dots with statistical error bars). The clusters were stored for 90 ms before they were subjected to the laser pulse. The solid (red) curves are the result of a fit of the experimental data with Eq. (11) by varying the photo-destruction cross section σ_0. The results for σ_0 are given with their statistical errors.

Examples of depletion curves observed for Al_3^- and Al_5^- clusters, induced after a storage time of 90 ms by a laser pulse with 2.25 eV photons (λ = 550 nm), are shown in Fig. 6. The variance of the laser beam profile was determined before and after the measurements to be $\sigma_{ph} = (0.70 \pm 0.15)$ mm. Moreover, to limit the dead time correction to about 10% (see Sec. II E), the number of clusters stored per injection was adjusted such that the number of particles N_b measured per spill was kept around $N_b = 30$. Note that the linear increase of D at small U is consistent with the expectation that the destruction occurs by a one-photon absorption (see also below).

The total destruction cross sections σ_0 are extracted from the measured depletion curves $D(U)$ by comparing them to calculated curves based on measured and simulated properties of our setup. To calculate these curves, we first consider the probability $p(z, r, \varphi; U)$ to find a cluster at the position (z, r, φ) after the laser pulse. This probability is given by

$$p(z, r, \varphi; U) = p(z, r; U) = \rho(z, r) \exp(-\sigma_0 N_{ph}(U) f(r)), \tag{10}$$

where $\rho(z, r)$ is the probability to find the cluster at the position (z, r, φ) before the laser pulse (see Sec. II B), N_{ph} denotes the number of photons in the laser pulse, and $f(r)$ is the

normalized area density of the photons introduced in Sec. II C. In writing Eq. (10), we made use of the fact that (i) N_{ph} is very much larger than the number of ions stored in the trap, which allows neglecting the absorption of photons by the ions, and (ii) the laser pulse length is much smaller than the oscillation time such that the clusters can be considered to be stationary during the laser pulse. Moreover, we assumed that the absorption of a single photon leads to the destruction of the cluster.

Integrating over the storage volume of the trap, we then obtain for the depletion probability $D(U)$, taking into account that $\iiint \rho(z,r)dzrdrd\varphi = 1$ when integrated over the trap volume,

$$D(U) = 1 - P(U) = 1 - 2\pi \int_0^\infty \int_0^{z_c^+} p(z,r;U)dz\,r\,dr$$
$$-2\pi \int_0^{r_0} \int_{z_c^-}^0 p(z,r;U)dz\,r\,dr - 2\pi \int_{r_0}^\infty \int_{z_c^-}^0 \rho(z,r)dz\,r\,dr \tag{11}$$

with r_0 being the radius of the deflector hole, and z_c^-, z_c^+ denoting the turning points of the stored particles in the trap mirrors. Note that the second line in Eq. (11) takes into account that the laser beam profile is truncated by the deflector for $z < 0$ such that clusters at $r > r_0$ are not subjected to the laser photons; it is obvious from Fig. 2, however, that the contribution of the latter term to $D(U)$ is small so that for intense enough laser pulses depletion probabilities close to unity can be reached.

The solid (red) curves plotted in Fig. 6 are the results of a χ^2 fit of the measured depletion curves using Eq. (11) with σ_0 being the only free parameter. The absolute errors of ± 0.05 Å^2 comprise the statistical errors as well as the uncertainties observed when changing the fitting range. The sensitivity of the deduced σ_0 to the width of the laser beam is surprisingly small; restricting the fit to $D \lesssim 0.9$ the deduced cross sections turn out to be stable to within 2% when varying the variance of the laser profile within its experimental limits.

The largest systematic uncertainty in the measurement of the destruction cross section via depletion seems to be connected with the precise alignment of the laser beam along the trap axis and all the way up to the photo diode located behind the switching magnet. Deviations of the deduced cross sections of as large as 20% have been observed when comparing measurements performed on different days after a complete shut-down. In view of these reproducibility uncertainties, we estimate the overall accuracy of the deduced absolute cross sections to be about 20%–25%, while for relative cross sections accuracies can be reached which are mainly determined by statistical issues to $\lesssim$10%. We thus obtain from the two measurements shown in Fig. 6

$$\sigma_0(550\,\text{nm}) = (0.80 \pm 0.17)\,\text{Å}^2 \text{ for } Al_3^-,$$
$$\sigma_0(550\,\text{nm}) = (0.39 \pm 0.09)\,\text{Å}^2 \text{ for } Al_5^-.$$

A word of caution is in place about the interpretation of the cross section measured by depletion. In the two cases investigated, where the photon energy of 2.25 eV is above the (vertical) electron detachment energy and above the one-atom fragmentation energy even for ground state Al_3^- and Al_5^-,[16] the absorption of a single photon is already sufficient to cause the destruction of the cluster. Thus the destruction cross section can be deduced from the measured depletion with the aid of Eqs. (10) and (11) and taken as a good measure of the photon absorption cross section. The interpretation of depletion curves can be readily extended to cases where, e.g., the absorption of two photons is required to cause destruction. Within the usual assumption that the photon absorption cross sections of both steps are the same and given by σ_0, Eq. (10) has to be replaced by

$$p(z,r;U) = \rho(z,r)(1 + \sigma_0 N_{ph}(U) f(r)) \exp(-\sigma_0 N_{ph}(U) f(r)). \tag{12}$$

Since a one-photon absorption process leads to a linear dependence of the depletion curve $D(U)$ for small values of U while a quadratic dependence of $D(U)$ is connected with a two-photon absorption process, both cases can be readily distinguished if one of the processes is dominating the destruction of the stored cluster ensemble. However, in case both processes are of equal importance, a precise measurement of the U dependence of the depletion function is required to recognize even two-photon contributions as large as 50% on top of the one-photon contribution.

IV. TOTAL PHOTO-INDUCED FRAGMENTATION CROSS SECTIONS

To exemplify the use of the present setup to determine the total fragmentation cross sections σ_f, or rather the total branching ratio $b_f = \sigma_f/\sigma_0$ for fragmentation, we shall use the case of Al_5^- clusters excited after 90 ms of storage by a laser pulse with $\lambda = 550$ nm photons. The photon energy of 2.25 eV is larger than the adiabatic binding energy of the electron, calculated to be 2.06 eV, and also larger than the binding energy of an Al-atom in Al_5^- of 2.22 eV, but considerably smaller than the calculated binding energy of a dimer of 3.36 eV and the threshold energies of the $m = 3, 4$ channels.[16]

For an overview of which of the possible fragmentation channels

$$Al_5^- + \hbar\omega \rightarrow Al_{5-m}^- + Al_m \tag{13}$$

are actually observable, a fragment mass spectrum was measured by scanning the deflector voltage, subjecting the Al_5^- clusters to laser pulses of 0.2 mJ. While fragmentation products with $m = 3, 4$ were not observed (<0.5% as compared to the monomer product Al_4^-), we unexpectedly detected a sizable amount of Al_3^- fragments. This is surprising in view of the high threshold energy for dimer emission and the absence of this fragmentation channel in an earlier study performed at even higher photon energies.[17] However, as we will show below, the appearance of Al_3^- in the present experiment is predominantly due to the destruction of the monomer product Al_4^- by the absorption of an additional photon from the laser pulse rather than the emission of an Al_2 dimer.

A. Monomer fragmentation

Let us first consider the Al_4^- channel ($m = 1$). We measure the appearance of the Al_4^- daughter and "simultaneously" the depletion of Al_5^- by switching for three consecutive injections the deflector voltage first to V_p about 1 ms before the laser pulse, then again to V_p about 1 ms after the pulse, and finally ~2.5 μs before the laser pulse (see Sec. II D) to the appropriate voltage V_{def} required to deflect the daughter fragments. As before, for a given laser pulse energy U, the cycle is repeated many times to smooth out fluctuation of the number of injected particles and to obtain sufficient statistics. Denoting the (dead time corrected) number of parent clusters detected before and after the laser pulse again by N_b and $N_a(U)$, respectively, and the number of detected $m = 1$ fragments by $N_{f1}(U)$, we can determine the appearance probability $P_{f1}(U)$:

$$P_{f1}(U) = \frac{N_{f1}(U)/\epsilon_{f1}}{N_b/\epsilon_p} = \frac{\epsilon_p N_{f1}(U)}{\epsilon_{f1} N_b} \tag{14}$$

and deduce a function $B_{f1}(U)$ defined by

$$B_{f1}(U) = \frac{P_{f1}(U)}{D(U)}, \tag{15}$$

which contains information about the branching ratio b_{f1}. For the present example the efficiency ratio entering Eq. (14) is $\epsilon_p/\epsilon_{f1} = 3.1 \pm 0.3$ (see Fig. 4 and Ref. 9).

The three functions $D(U)$, $P_{f1}(U)$, and $B_{f1}(U)$, observed when illuminating Al_5^- with photons of $\lambda = 550$ nm, are displayed in Fig. 7. The pulse energy dependence of the appearance probability $P_{f1}(U)$ clearly reveals that the probability for producing an Al_4^- fragment does not saturate but goes through a maximum and decreases with increasing laser power. Two processes could in principle be responsible for this observation: (i) A second photon is absorbed by the Al_5^- cluster before it has a chance to decay, thereby leading to excitation energies high enough to open up other fragmentation channels. (ii) The nascent Al_4^- fragment is destroyed by absorbing another photon from the laser pulse. As the emission of an electron or atom is energetically allowed already after the absorption of a single photon, the largely different time scales between "prompt" decays ($\lesssim$1 ps) and the length of the laser pulse (9 ns) renders the second process to be considerably more likely. For clarity, the following discussion will be based on the latter scenario, although we will show that the extraction of the branching ratio b_{f1} will not be affected by this assumption.

Within this scenario the probability to find a daughter fragment at position (z, r, φ) in the trap after the laser pulse is found to be, following the reasoning leading to Eq. (10),

$$p_{f1}(z, r; U) = b_{f1} \frac{\sigma_0}{\sigma_0 - \sigma_{d1}} (p_{d1}(z, r; U) - p_0(z, r; U)) \tag{16}$$

with

$$p_i(z, r; U) = \rho(z, r) \exp(-\sigma_i N_{ph}(U) f(r)), \tag{17}$$

and σ_{d1} denoting the destruction cross section of the daughter fragment $f1$. For the appearance probability $P_{f1}(U)$, we thus obtain

$$P_{f1}(U) = b_{f1} \frac{\sigma_0}{\sigma_0 - \sigma_{d1}} (\hat{P}_{d1}(U) - \hat{P}_0(U)) \tag{18}$$

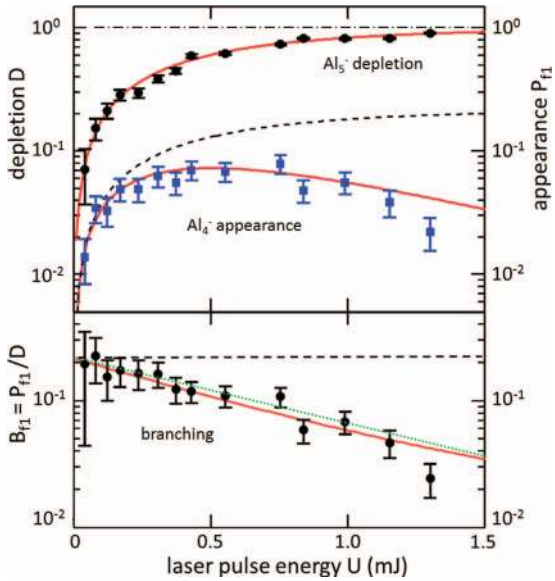

FIG. 7. Measured pulse energy dependence (symbols with statistical error bars) of the depletion probability $D(U)$ of Al_5^- and the appearance probability $P_{f1}(U)$ of Al_4^- (upper panel), and of the corresponding branching function $B_{f1}(U)$ (lower panel). The data were observed when illuminating Al_5^- clusters after 90 ms of storage by a short laser pulse with $\lambda = 550$ nm photons. The solid (red) lines are calculated probabilities including the destruction of the nascent Al_4^- by the absorption of a photon from the same laser pulse (see main text). The thick dashed lines indicate the expected pulse energy dependences of $P_{f1}(U)$ and $B_{f1}(U)$ in the absence of the daughter destruction channel. The dotted (green) curve is an exponential fit of $B_{f1}(U)$ to extrapolate the data to $U = 0$.

with

$$\hat{P}_i(U) = \frac{2\pi \int_0^{r_0} \int_{z_d^-}^{z_e^-} p_i(z, r; U) dz\, r dr}{2\pi \int_0^{\infty} \int_{z_d^-}^{z_e^-} \rho(z, r) dz\, r dr}, \tag{19}$$

where we took explicitly care of the fact that only fragments created between position z_d^- and z_e^- can be detected (see Sec. II D and Fig. 4). The branching function $B_{f1}(U)$ is then finally obtained by dividing $P_{f1}(U)$ by $D(U)$ given by Eq. (11).

As displayed in Fig. 7 by the solid lines, the measured appearance probability and branching function can be well reproduced within this scenario by using the destruction cross section $\sigma_0 = 0.39$ Å^2 determined in Sec. III and by adjusting the branching ratio b_{f1} and the total destruction cross section σ_{d1} of the nascent Al_4^- to $b_{f1} = 0.22$ and $\sigma_{d1} = 0.45$ Å^2. The deduced daughter cross section σ_{d1}, estimated to be accurate to within 20%, turns out to be about a factor of two larger than the destruction cross section observed for Al_4^- clusters stored for 90 ms prior to the laser pulse. Although reasonable, it remains to be seen if the higher destruction cross section can be attributed to the nascent Al_4^- fragment being considerably hotter.

Despite the successful description of the data within this scenario, we would like to point out that the branching ratio b_{f1} can be directly deduced from the data without having to rely on a specific model to account for the loss of Al_4^- fragments at high laser powers. Expanding the appearance probability $P_{f1}(U)$ and the depletion function $D(U)$ given by Eqs. (18) and (11), respectively, for small pulse energies U

one finds that the branching function $B_{f1}(U)$ reduces to

$$B_{f1}(U) \to b_{f1}\frac{F_f}{F_0} \tag{20}$$

in the limit of $U \to 0$, where the overlap factors F_f and F_0 are given by

$$F_f = \frac{2\pi \int_0^{r_0}\int_{z_d^-}^{z_e^-} \rho(z,r) f(r) dz\, r dr}{2\pi \int_0^{\infty}\int_{z_d^-}^{z_e^-} \rho(z,r) dz\, r dr} \tag{21}$$

and

$$F_0 = 2\pi \int_0^{\infty}\int_0^{z_c^+} \rho(z,r) f(r) dz\, r dr + 2\pi \int_0^{r_0}\int_{z_c^-}^{0} \rho(z,r) f(r) dz\, r dr. \tag{22}$$

The ratio of the two overlap factors is close to unity for all reasonable laser beam widths; for $\sigma_l = 0.7$ mm, e.g., one obtains $F_f/F_0 = 0.93$.

We can thus deduce the branching ratio b_{f1} by extrapolating the branching function $B_{f1}(U)$ to $U = 0$, whereby the extrapolation is preferentially done by an experimental fit to the data as shown in Fig. 7. Taking the ratio $F_f/F_0 = 0.93$ into account we thus obtain for the branching ratio of laser excited ($\lambda = 550$ nm) Al_5^- into the monomer channel

$$b_{f1} = 0.23 \pm 0.03,$$

where the error comprises the statistical error as well as the uncertainties connected with the efficiency correction.

When deriving the collection efficiencies for fragments, we assumed that the fragmentation occurs "promptly," that is in times after the laser pulse that are short compared to the inherent time resolution of our setup (2.6 μs in the present case, see Sec. II D). The validity of this assumption can be verified by delaying the switching the deflector voltage relative to the laser pulse. Delayed fragmentations occurring outside the "prompt" time window were estimated in this way to be less than 1% of the "prompt" yield.

B. Dimer fragmentation

The deflector voltage scan performed at a laser pulse energies of 0.2 mJ revealed that also Al_3^- fragments were produced when subjecting Al_5^- to 550 nm photons. In view of the large binding energy of an Al_2 cluster in Al_5^- of 3.36 eV,[16] it is very unlikely that the absorption of a single photon of energy 2.25 eV by an Al_5^- stored and cooled down for 90 ms after production is sufficient to lead to the emission of a dimer. It is considerably more likely that two-phonon processes are responsible for the occurrence of Al_3^- products. As we have shown in Subsection IV A that the observed pulse energy dependence of the $m = 1$ fragmentation channel can be successfully described by assuming the nascent Al_4^- fragment to be partly destructed by absorbing another photon from the laser pulse, we can indeed expect that the destruction of the Al_4^- fragments occurs at least partly also by the emission of a monomer and thus to contribute to the production of Al_3^-. We will refer to this destruction path as the monomer-monomer (mm) channel.

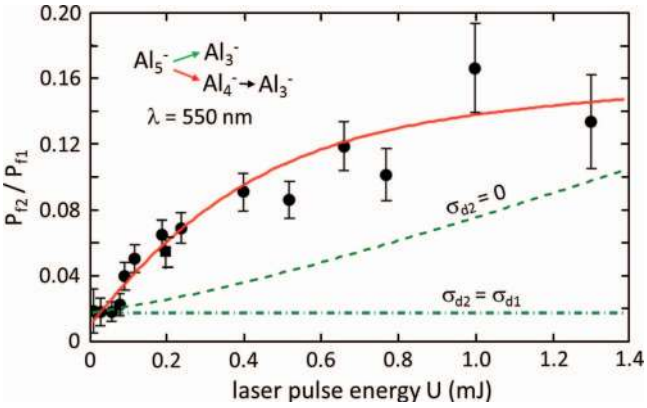

FIG. 8. Appearance probability of Al_3^- observed relative to that of Al_4^- when subjecting Al_5^- after 90 ms of storage to a 9 ns long pulse of 550 nm photons (full circles, with error bars reflecting statistical uncertainties). The (green) dashed and (green) dashed-dotted lines are expected pulse energy dependences of the probability ratio in case the appearance of Al_3^- would be solely due to a one-photon induced dimer decay of Al_5^-, assuming two extreme values for the secondary destruction cross section σ_{d2} of Al_3^-. The (red) solid curve is obtained by allowing also for the production of Al_3^- by the photo-induced fragmentation of the nascent Al_4^- (for more details see main text).

To further investigate the origin of the Al_3^- products, the Al_3^- yield was measured as a function of the laser pulse energy. To avoid the normalization to the number of stored ions per injection, which is limited due to dead time considerations (see Sec. II E), the Al_3^- yield was measured relative to that of Al_4^- fragments by recording alternately the number of Al_3^- and Al_4^- fragments $N_{f2}(U)$ and $N_{f1}(U)$, respectively, integrating over 200 injections per U. Correcting for the slightly different detection efficiencies, we can thus deduce the probability ratio $R_{2,1}(U)$ by

$$R_{2,1}(U) = \frac{P_{f2}(U)}{P_{f1}(U)} = \frac{\epsilon_{f1}}{\epsilon_{f2}}\frac{N_{f2}(U)}{N_{f1}(U)} \tag{23}$$

describing the appearance of Al_3^- relative to that of Al_4^-. The result is displayed in Fig. 8 using an efficiency ratio of $\epsilon_{f1}/\epsilon_{f2} = \epsilon_{f1}^{rec}/\epsilon_{f2}^{rec} = 1.1 \pm 0.1$ (see Ref. 9).

We first discuss the pulse energy dependence expected for dimer ($m = 2$) decay of Al_5^- after the absorption of a single photon. Following the reasoning leading to Eq. (18), we find

$$R_{2,1}^{dim}(U) = \frac{b_{f2}}{b_{f1}}\frac{(\sigma_0 - \sigma_{d1})}{(\sigma_0 - \sigma_{d2})}\frac{(\hat{P}_{d2}(U) - \hat{P}_0(U))}{(\hat{P}_{d1}(U) - \hat{P}_0(U))} \tag{24}$$

with $b_{f2} = \sigma_{f2}/\sigma_0$ denoting the dimer branching ratio, and σ_{d2} the destruction cross section of the nascent Al_3^-. Applying Eq. (24) to the data displayed in Fig. 8, using values deduced in Sec. IV A for the destruction cross section σ_0, the branching ratio b_{f1}, and the secondary destruction cross section σ_{d1} of the nascent Al_4^-, no satisfactory description can be reached by varying b_{f2} and σ_{d2}. Even for the unrealistic case of $\sigma_{d2} = 0$, a one-photon induced dimer decay of Al_5^- cannot reproduce the observed pulse energy dependence of the appearance ratio.

Next we include the possible contribution from the monomer-monomer channel in the appearance ratio. This

can be readily achieved by replacing Eqs. (16)–(18) by the corresponding formulae which take into account the parent-daughter-granddaughter decay chain. Denoting the branching ratio for monomer fragmentation of the laser excited intermediate Al_4^- fragment by b_{mm}, and keeping the previously determined values for σ_0, b_{f1}, and σ_{d1}, a reasonable and consistent description of the data is obtained assuming $\sigma_{d2} \approx \sigma_{d1}$ and choosing $b_{mm} \approx 0.13$ and $b_{f2} \approx 0.002$ (see solid (red) line in Fig. 8).

Finally we notice that the monomer-monomer contribution, as any other two-photon contribution to the appearance probabilities, extrapolates to 0 for $U \to 0$, while the dimer ratio reduces to $R_{2,1}^{dim}(U) = b_{f2}/b_{f1}$. We can thus deduce the dimer branching ratio b_{f2} by extrapolating the measured ratio to $U = 0$. From the data shown in Fig. 8, we thus obtain for the m = 2 decay channel of laser excited ($\lambda = 550$ nm) Al_5^-,

$$b_{f2} \lesssim 0.004.$$

The absence of dimer emission is in line with earlier findings of Saunders *et al.*[17] and the vain attempts to even observe delayed dimer emission in small Al_n^- clusters.[18]

C. Total fragmentation and detachment cross sections

Combining the results of Subsections IV A and IV B, we obtain for the total fraction b_f of Al_5^- clusters dissociating according to Eq. (13) when excited by a laser pulse with $\lambda = 550$ nm photons

$$b_f = \sum\nolimits_m b_{fm} = 0.23 \pm 0.03,$$

and thus for the corresponding fraction b_e of laser-excited Al_5^- decaying by electron detachment

$$b_e = 1 - b_f = 0.77 \pm 0.03.$$

Together with the total photo-destruction cross section of $\sigma_0 = (0.39 \pm 0.09)$ Å^2 determined in Sec. III, we thus obtain for the total photo-fragmentation cross section

$$\sigma_f = (0.09 \pm 0.03)\,\text{Å}^2,$$

and

$$\sigma_e = (0.30 \pm 0.09)\,\text{Å}^2$$

for the total photo-induced electron-detachment cross section.

V. CONCLUSION

The bent electrostatic trap has been shown to be a versatile tool for investigating laser induced decays of small cluster anions. In the bent configuration, where the ions are kept oscillating on V-shaped trajectories by the electrostatic deflector, the clusters can be overlapped in one arm of the V by a laser pulse, while photo-induced delayed decay products can be detected in the second arm. This configuration is in particular suited for measuring the competition between delayed monomer fragmentation and delayed electron detachment as described in Refs. 9 and 10. In the linear configuration investigated in the present work, the comprehensive overlap of the stored ions by the laser pulse allows the measurement of the total (sum of prompt and delayed) absolute destruction cross section by depletion and the measurement of the branching ratios for all fragment channels, using the deflector to mass-selectively detect either the surviving parent clusters or the charged dissociation products. Thus total absolute fragmentation and electron-detachment cross sections can be determined. In summary, the two configurations the bent EIBT can be operated in provide a comprehensive access to the properties of photo excited clusters.

The analysis of the depletion curves measured in the present feasibility study was performed under the presupposition that the absorption of a single photon is sufficient to cause the destruction of the cluster. The assumption implies that the absorption of a second photon from the laser pulse does not influence the destruction probability. However, the depletion measurements and their analysis can be readily extended to cases where only a two- (or a n-) photon process is leading to the destruction of the stored cluster ensemble. In these cases, the branching ratios into the various fragmentation channels can be deduced in a straightforward way by extrapolating the appearance probability, normalized to the depletion probability or to the appearance probability of the most prominent fragmentation product, to zero pulse energies. The situation gets more involved if at the same time one- and two-photon processes are occurring, in particular, the recognition that both processes are contributing to the depletion curve requires a very careful study of its pulse energy dependence.

Absolute cross sections can be measured in this setup for X_n clusters with $n \lesssim 20$, the limitation being due to the mass resolution that can be achieved by the deflection technique, which depends on the focusing/defocusing properties of the electrostatic deflector and on the divergence of the trajectories of the stored ions. The uncertainties of the deduced branching ratios and relative cross sections are mainly determined by statistical issues and can be kept below ~15%, while accuracy of absolute cross sections is limited by systematic uncertainties to about 20%−25%, which seem to be mainly connected with the alignment of the laser beam through the 3 mm hole of the deflector.

Improvements are conceivable when considering the construction of a dedicated EIBT setup optimized for these purposes: By increasing the diameter of the central hole in the deflector by a factor of two and by reducing the length of the straight section between the switching magnet and the trap, the alignment of the laser beam along the axis of the setup would be considerably facilitated. Moreover, in view of the output power of modern lasers, the laser beam waist could be increased without hampering the depletion measurements, but with the advantage of an overlap region being less sensitive to the precise alignment of the two merged beams. These measures should considerably improve the reproducibility of the results, which, in the present setup, is limiting the absolute accuracy of the cross section measurements.

ACKNOWLEDGMENTS

This work has been supported by the Israeli Science Foundation (Grant No. 124/09), and by a research grant from the estate of David Turner. D.Sch. acknowledges support by

the Weizmann Institute of Science through the Joseph Meyerhoff program.

[1]D. Zajfman, O. Heber, L. Vejby-Christensen, I. Ben Itzhak, M. Rappaport, R. Fishman, and M. Dahan, Phys. Rev. A **55**, R1577 (1997).
[2]M. Dahan, R. Fishman, O. Heber, M. Rappaport, N. Altstein, D. Zajfman, and W. J. van der Zande, Rev. Sci. Instrum. **69**, 76 (1998).
[3]L. H. Andersen, O. Heber, and D. Zajfman, J. Phys. B **37**, R57 (2004).
[4]M. Lange, M. Froese, S. Menk, J. Varju, R. Bastert, K. Blaum, J. R. Crespo Lpez-Urrutia, F. Fellenberger, M. Grieser, R. von Hahn, O. Heber, K.-U. Khnel, F. Laux, D. A. Orlov, M. L. Rappaport, R. Repnow, C. D. Schrter, D. Schwalm, A. Shornikov, T. Sieber, Y. Toker, J. Ullrich, A. Wolf, and D. Zajfman, Rev. Sci. Instrum. **81**, 055105 (2010).
[5]C. J. Johnson and R. E. Continetti, J. Phys. Chem. Lett. **1**, 1895 (2010).
[6]J. B. Greenwood, O. Kelly, C. R. Calvert, M. J. Duffy, R. B. King, L. Belshaw, L. Graham, J. D. Alexander, I. D. Williams, W. A. Bryan, I. C. E. Turcu, C. M. Cacho, and E. Springate, Rev. Sci. Instrum. **82**, 043103 (2011).
[7]M. Hass, S. Vaintraub, O. Aviv, K. Blaum, O. Heber, I. Mardor, M. Rappaport, A. Wolf, and D. Zajfman, J. Phys.: Conf. Ser. **267**, 012013 (2011).
[8]O. Heber, R. Golser, H. Gnaser, D. Berkovits, Y. Toker, M. Eritt, M. L. Rappaport, and D. Zajfman, Phys. Rev. A **73**, 060501R (2006).
[9]O. Aviv, Y. Toker, M. Errit, K. G. Bhushan, H. B. Pedersen, D. Strasser, M. L. Rappaport, O. Heber, D. Schwalm, and D. Zajfman, Rev. Sci. Instrum. **79**, 083110 (2008).
[10]O. Aviv, Y. Toker, D. Strasser, M. L. Rappaport, O. Heber, D. Schwalm, and D. Zajfman, Phys. Rev. A **83**, 023201 (2011).
[11]B. Kafle, O. Aviv, V. Chandrasekaran, O. Heber, M. L. Rappaport, D. Schwalm, D. Strasser, Y. Toker, and D. Zajfman, "Absolute electron-detachment and fragmentation cross-sections for laser excited Al_4^- anions" (unpublished).
[12]D. Zajfman, D. Strasser, O. Heber, S. Goldberg, A. Diner, and M. L. Rappaport, Nucl. Instrum. Methods Phys. Res. A **532**, 196 (2004).
[13]See www.simion.com for a description of the simulation program.
[14]H. B. Pedersen, D. Strasser, O. Heber, M. L. Rappaport, and D. Zajfman, Phys. Rev. A **65**, 042703 (2002).
[15]G. F. Knoll, *Radiation Detection and Measurement* (Wiley & Sons, 1979), pp. 95–99.
[16]B. K. Rao and P. Jena, J. Chem. Phys. **111**, 1890 (1999).
[17]W. A. Saunders, P. Fayet, and L. Wöste, Phys. Rev. A **39**, 4400 (1989).
[18]O. Aviv, Y. Toker, J. Rajput, D. Strasser, O. Heber, D. Schwalm, D. Zajfman, and L. Andersen, Phys. Rev. A **82**, 035201 (2010).